*Korean J. Chem. Eng.*, 34(5), 1319-1327 (2017)
DOI: 10.1007/s11814-017-0022-4

pISSN: 0256-1115
eISSN: 1975-7220

# Nanoparticle deposition in transient gaseous microchannel flow considering hindered motion and rarefaction effect

**Salahaddin Andarwa and Hassan Basirat Tabrizi†**

Department of Mechanical Engineering, Amirkabir University of Technology, P. O. Box 15875-4413, Tehran, Iran
(*Received 13 October 2016 • accepted 6 February 2017*)

**Abstract**−Interaction between wall and flow becomes more important when the scale of a channel decreases. We investigated two effects of wall presence for the transport of nanoparticle in a microchannel, which are the rarefaction effect up to early transient regime and hindered motion of nanoparticles. Lattice Boltzmann method coupled with Lagrangian nanoparticle tracking was used for modeling. Series of numerical simulation for various nanoparticle diameters, channel geometries, fluid velocities, and Knudsen numbers were performed. Some important features on nanoparticle transport such as capture efficiency, deposition velocity and deposition location were discussed. Using suitable dimensionless parameters, correlations for capture efficiency and deposition velocity were obtained. Considering hindered motion leads to significant decrease in the capture efficiency and deposition velocity. Results show that the effect of rarefaction on deposition is mostly because of varying the force acting on nanoparticles not due to slip velocity of fluid field near boundaries.

Keywords: Nanoparticle, Microchannel, Deposition, Lattice Boltzmann Method, Correlation

## INTRODUCTION

Microfluidics deals with the flow of fluids and of suspensions in submillimeter sized systems. These miniaturized fluidic systems are regarded as one of the most promising technologies and attracted many researchers from many disciplines. Two-phase gas-nano/micro particle flow is an interesting case of these studies. This category can be found in nature or in industrial applications, such as flow in the pulmonary passages [1-3], microsized fluidized beds, microreactors, micromixers, and filters [4]. Lab-on-a-chip systems can be optimized in microsize scale in application. Efficient mixing and rapid chemical reaction at the nanoliter to picoliter scales allow microfluidic devices to better control the synthesis parameters, and thus the nanoparticle sizes and properties [5]. In fact, generating, mixing, and handling of nanoparticles are in principle feasible for microchannels [6].

Clogging or totally blockage of microchannels due to the adhesion of small particles to the channel walls is a serious problem in many applications such as contaminant clogging of microchannels in micro-electro-mechanical systems (MEMS) devices, microchannels used for nanoparticle processing and dispersion devices [7]. In addition, deposition is an interesting factor in grooved filters. Such problems necessitate the study of methods for predicting and describing nanoparticle deposition in microchannels.

Gas-nanoparticle flow in microchannels has some issues, which should be considered, e.g., selecting a suitable solver for determining the hydrodynamics of this kind of flow is important. A solver should be able to resolve non-equilibrium effects in a widespread Knudsen number. Further, because of the complex geometry of many micromixers and microreactors, may be necessary for effective mixing or sorting and counting [8]; the solver should be able to resolve the problem easily. Lattice Boltzmann method (LBM) is promising as an alternative nonconventional technique for applications in computational fluid dynamics (CFD) to cover both necessities and can be considered as one of the best candidates for this category. In addition, in the vicinity of walls boundaries, the diffusion tendency of nanoparticles can be affected by the wall known as hindered diffusion.

Some studies have been reported for fluid-particle flow in a microchannel, e.g., Ansari et al. [9] investigated the motion and deposition of solid particles in regular and irregular structure filters using LBM-LAG approach. Basagaoglu et al. [10] analyzed particle migration under a creeping flow regime in a microchannel with a series of constricted passages imposed by rectangular channel wall obstacles experimentally and numerically. Afshar et al. [11] investigated dispersion of nanoparticles in a microchannel in slip regime using velocity and temperature profile. They concluded that nanoparticle deposition decreased when nanoparticle diameter and pressure drop increased.

In some studies, the hindered motion has been included. Andarwa et al. [12] studied the importance of hindered motion in their analysis. They introduced a criterion of importance for considering such an effect in capture efficiency. They modified Li and Ahmadi [13] formulation for Brownian motion to account for the hindered motion. Michaelides [14] investigated the effect of hindered diffusion on the thermophoretic motion of the nanoparticles in stagnant fluid near the horizontal plane wall. It was indicated the motion toward the wall is significantly retarded because of the

†To whom correspondence should be addressed.
E-mail: hbasirat@aut.ac.ir

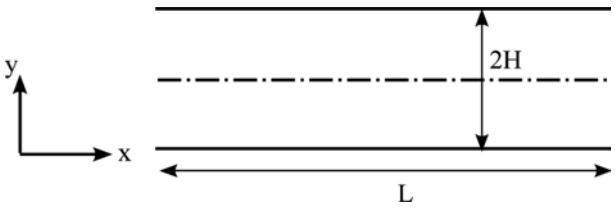


**Fig. 1. Schematic of the geometry and the parameters of a microchannel.**

drag enhancement. Katelhon et al. [15] included hindered diffusion in the modeling of interface-based sensors. They indicated the importance of considering hindered motion in sensor response.

Despite many researches on particle deposition in channels [16, 17], still some may be usable in the microchannel; this literature survey indicates that there is no correlation and study in detail for capture efficiency and deposition velocity in a gaseous microchannel flow considering both early transient regime and hindered diffusion of nanoparticles. Therefore, this study sought the aforementioned problem via LBM-LAG method. The LBM solver is able to cover flow field up to early transient regime.

## ANALYSIS

### 1. Geometry

Incompressible two-dimensional flow containing nanoparticles between two parallel plates with the channel width of 2H and length of L is considered (see Fig. 1). There are different methods for simulation of colloidal dispersion [18]. We applied a hybrid computational approach that combines LBM for flow field with a LAG scheme for the nanoparticles.

In gas-nanoparticle flow, two Knudsen numbers are defined; the flow Knudsen that is $Kn=\lambda/2H$, where $\lambda$ is the gas mean free path, reflects rarefaction effects of the gas flow in the microchannel, and particle Knudsen number, $Kn_p=2\lambda/d_p$, where is the particle diameter, accounts flow for the rarefied flow around nanoparticles. Roughly $Kn<0.001$, $0.001<Kn<0.1$ and $0.1<Kn<10$, respectively, correspond to continuum, slip and transient regimes [19].

### 2. LBM for Carrier Phase

The LBM has been successful for microscale gas flows and has attracted significant research interest. Commonly for microscale flow, LBM based on standard Bhatnagar-Gross-Krook (BGK) is coupled with appropriate relaxation time model to resolve Knudsen layer effect in transition regime [20]. The LBM with single-relaxation-time combined with BGK collision operator is given [21]:

$$f_\alpha(x+c_\alpha\Delta t,\ t+\Delta t)-f_\alpha(x,\ t)=\frac{1}{\tau}[f_\alpha^{eq}(x,\ t)-f_\alpha(x,\ t)] \tag{1}$$

where $f_\alpha(x,\ t)$ is fluid particle probability density distribution function. It represents the probable amount of fluid particles moving with a fixed velocity $c_\alpha$ along the $\alpha$ direction at each node with position and at discrete time. $\tau$ is the single relaxation time parameter that controls the rate of approach to equilibrium. Each $f_\alpha$ corresponds to a certain velocity vector $c_\alpha$ that for D2Q9 (see Fig. 2) lattice model are:

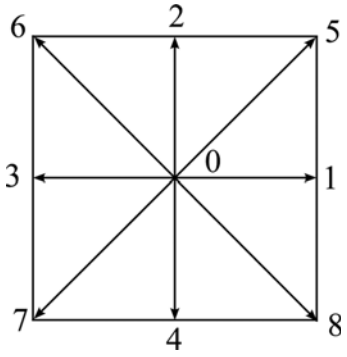


**Fig. 2. Schematics of the D2Q9 lattice models.**

$$c_\alpha=\begin{cases}(0,\ 0) & \alpha=0\\ c(\cos[(\alpha-1)\pi/2],\ \sin[(\alpha-1)\pi/2]) & \alpha=1,\ 2,\ 3,\ 4\\ \sqrt{2}c(\cos[(2\alpha-1)\pi/4],\ \sin[(2\alpha-1)\pi/4]) & \alpha=5,\ 6,\ 7,\ 8\end{cases} \tag{2}$$

In which $c=\Delta x/\Delta t$ that $\Delta x$ is the grid length. The equilibrium distribution for D2Q9 model is:

$$f_\alpha^{eq}=\rho\omega_\alpha\left[1+\frac{\mathbf{c}_\alpha\cdot\mathbf{u}}{c_s^2}+\frac{1}{2}\left(\frac{\mathbf{c}_\alpha\cdot\mathbf{u}}{c_s^2}\right)^2-\frac{(\mathbf{u}\cdot\mathbf{u})^2}{2c_s^2}\right],\ \omega_0=\frac{4}{9};$$
$$\omega_\alpha=\frac{1}{9}\alpha=1,\ 2,\ 3,\ 4;\ \omega_\alpha=\frac{1}{36}\alpha=5,\ 6,\ 7,\ 8 \tag{3}$$

$c_s=\sqrt{3}\,c/3$ is the local speed of sound.

The macroscopic density, velocity and pressure of fluid can be calculated as:

$$\rho=\sum_0^{\alpha=8}f_\alpha,\ \mathbf{u}=\sum_0^{\alpha=8}f_\alpha\mathbf{c}_\alpha/\rho,\ P=\rho c_s^2 \tag{4}$$

The relaxation time is related to fluid kinematic viscosity as:

$$\nu=\frac{c_s^2}{2}(2\tau-1)\Delta t \tag{5}$$

This study considers the pressure-driven flow. Inlet and outlet is treated based on bounce back of the non-equilibrium distribution for unknown $f_\alpha$ [22]. The combination scheme of bounce back and specular reflection (BSR) is used for wall boundary [20,23]. Considering rarefaction in microchannel some correction should be applied on LBM to resolve microscale phenomena. Following Yue et al. [20] relaxation time is modified with the application on near wall effective mean free path. Auxiliary equations for closure are:

$$\lambda=\frac{\mu}{P}\sqrt{\frac{\pi RT}{2}},\ P=\rho RT,\ \mu=\frac{1.458\times10^{-6}T^{1.5}}{T+110.4} \tag{6}$$

where $\mu$ is fluid dynamic viscosity, R=287.058 J/kgK is the gas constant and T stands for temperature at Kelvin. For fluid dynamic viscosity, Sutherland's equation is used for analysis of flow in different temperature.

### 3. Forces Acting on Nanoparticles

Considered forces that act on nanoparticles are drag, Saffman lift, Brownian, van der Waals (vdW) and gravity. Using the Lagrangian tracking of nanoparticles, the governing equations are:

$$\frac{du_p^x}{dt}=F_D^x+F_B^x+F_{saffman}^x,\ \frac{dx_p}{dt}=u_p^x$$
$$\frac{du_p^y}{dt}=F_D^y+F_B^y+F_{saffman}^y+F_{vdW}+\left(\frac{\rho}{\rho_p}-1\right)g,\ \frac{dy_p}{dt}=u_p^y \quad (7)$$

where $x_p$, $y_p$ are particles positions and $u_p^x$, $u_p^y$ are particles translational velocities and $\rho_p$ stands for nanoparticles density. Details of force acting on nanoparticle including the wall effect are discussed in the following section.

3-1. Wall-presence Effect

Close to the wall, the drag and consequently diffusion needs to be corrected according to the direction of the particle motion; parallel or normal to the wall. The near wall correction to the Stokes-Cunningham drag is [24-27]:

$$C_{||}=\left(1-\frac{9}{16}\Delta^{-1}+\frac{1}{8}\Delta^{-3}-\frac{45}{256}\Delta^{-4}-\frac{1}{16}\Delta^{-5}\right)^{-1} \text{ for } \Delta\geq 2$$
$$C_{||}=\left(\frac{-2[\ln(\Delta-1)-0.9543]}{[\ln(\Delta-1)]^2-4.325\ln(\Delta-1)+1.591}\right)^{-1} \text{ for } \Delta<2 \quad (8)$$
$$C_{\perp}=\left[\frac{6(\Delta-1)^2+2(\Delta-1)}{6(\Delta-1)^2+9(\Delta-1)+2}\right]^{-1} \text{ where } \Delta=\frac{2z}{d_p}$$

where symbol z is the distance between the particle center and the nearest wall.

In the presence of two walls, linear superposition is applied for both parallel and normal motion as [28]:

$$C_{||}(I,II)\approx C_{||}(I)+C_{||}(II)-1,\ C_{\perp}(I,II)\approx C_{\perp}(I)+C_{\perp}(II)-1 \quad (9)$$

The wall effect is important for roughly up to 2.5 particle diameters away from the wall. The correction affects an area in flow cross section with a distance from each wall as $z\leq 2.5d_p$ which is called affected zone (AZ) [12]. Obviously, for greater affected zone (AZ) region, the wall effects become more dominant and the results will be more different in comparison with analysis with no wall effects.

3-2. Drag Forces

The components of the drag force per unit mass acting on a spherical particle are:

$$F_D^x=\frac{1}{\tau_p}C_{||}(u^x-u_p^x),\ F_D^y=\frac{1}{\tau_p}C_{\perp}(u^y-u_p^y) \quad (10)$$

where $\tau_p=d_p^2\rho_p C1_c(Kn_p)/18\mu$ and $C_c(Kn_p)$ are the relaxation time and Cunningham's slip correction factor, respectively. An empirical formula for slip correction factor based on the experimental study of Kim et al. [29] is used as:

$$C_c(Kn_p)=1+Kn_p\times\left(1.165+0.483\times\exp\left(-\frac{0.997}{Kn_p}\right)\right) \quad (11)$$

3-3. Brownian Forces

Based on Li and Ahmadi [13] the corresponding random Brownian force amplitudes per unit mass at each time step considering hindered diffusion was given [12]:

$$F_B^x=G^x\sqrt{\frac{\pi S_0^x}{\Delta t_p}},\ F_B^y=G^y\sqrt{\frac{\pi S_0^y}{\Delta t_p}} \quad (12)$$

where $G^x$, $G^y$ are selected from a population of zero-mean, unit variance independent Gaussian random numbers, and $\Delta t_p$ is the time step in the simulation. The corresponding spectral intensities including the anisotropic effects become:

$$S_0^x=\frac{216\mu k_b T}{\pi^2 d_p^5\rho_p^2 C_c(Kn_p)}C_{||},$$
$$S_0^y=\frac{216\mu k_b T}{\pi^2 d_p^5\rho_p^2 C_c(Kn_p)}C_{\perp} \quad (13)$$

Here $k_b$(=1.3805×10$^{-23}$ J/K), and $\rho_p$(=7870 kg/m$^3$) are, respectively, the Boltzmann constant and the nanoparticle density.

3-4. Lift and van der Waals Forces

Saffman's lift force per unit mass is given as [30,31]:

$$\vec{F}_{saffman}=1.615d_p^2(\rho\mu)^{0.5}\left(\frac{1}{|\omega|}\right)^{0.5}[(\mathbf{u}-\mathbf{u}_p)\times\omega] \quad (14)$$

where the fluid rotation is:

$$\omega=0.5\nabla\times\mathbf{u} \quad (15)$$

The interaction force between the nanoparticles and wall is the van de Waals force. The van der Waals force per unit mass of nanoparticle is [27]:

$$F_{vdW}=\frac{A_{pw}}{\pi\rho_p d_p^3}\left[-\frac{r_p}{(z-r_p)^2}-\frac{r_p}{(z+r_p)^2}+\frac{1}{(z-r_p)}-\frac{1}{(z+r_p)}\right] \quad (16)$$

where $A_{pw}$ is the Hamaker constant, z is wall to nanoparticle center distance and $r_p$ is the nanoparticles radius. Typically, a value of 1×10$^{-20}$ J for the Hamaker constant can be used.

## 4. Numerical Simulation

Simulation was performed by the method described in the previous section. As the flow field was obtained, nanoparticles were injected to the microchannel. For LBM simulation, the 20 lattice units were considered across the channel. Accuracy of flow field simulation in transient regime is controlled by comparison with

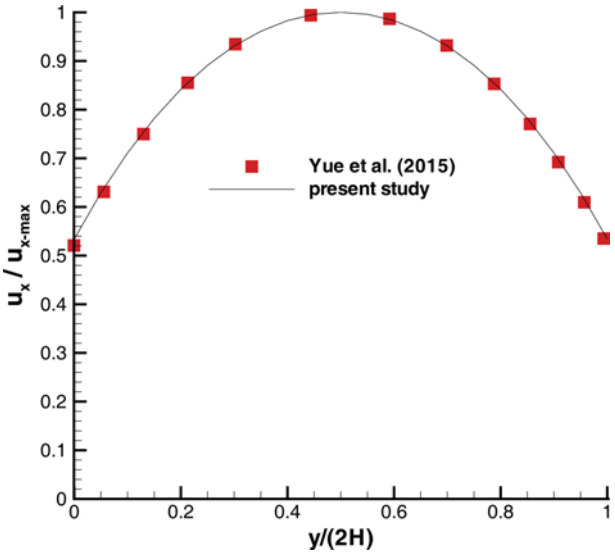


**Fig. 3. Flow velocity profile comparison of the present study with Yue et al. (2015) in output Knudsen number set to 0.388.**

**Table 1. Values of the parameters for various simulations**

| Case | L (mm) | 2H (μm) | T (K) | $P_{out}$/Patm | $U_{ave}$ (m/s) | $d_p$ (nm) |
|---|---|---|---|---|---|---|
| 1 | 1 | 4 | 300 | 1 | 0.79 | 30, 50, 100, 200, 300 |
| 2 | 1 | 4 | 300 | 1 | 0.079, 0.39, 0.79, 1.98, 3.96 | 75 |
| 3 | 1 | 4 | 300 | 1 | 0.079, 0.79, 3.96 | 250 |
| 4 | 0.25 | 1 | 300 | 0.2, 0.5, 1.8 | 0.79 | 100 |
| 5 | 1 | 4 | 150 | 1 | 0.79 | 50, 100, 200, 300 |
| 6 | 1 | 8 | 300 | 1 | 0.79 | 50, 100, 150, 250 |
| 7 | 2 | 4 | 300 | 1 | 0.79 | 30, 100, 150, 250 |
| 8 | 0.5 | 4 | 300 | 1 | 0.79 | 30, 100, 150, 250 |

Yue et al. [20] as seen in Fig. 3 wherein 20×2000 meshes were considered across and along the channel, respectively. The maximum difference between the results is below of 2%. The outlet Knudsen number was set as 0.388.

Typically, an ensemble of 100000 nanoparticles is injected into the microchannel. The particles are distributed uniformly across the channel inlet. Considered entrance velocity for nanoparticles is equal to the local fluid velocity. The nanoparticles are tracked until they are deposited on the walls or have exited from the channel. Deposition occurs while the distance of the particle center to the wall is equal to or less than its radius. To resolve the fluid velocity in the particle positions, a linear interpolation scheme was used. The trajectory, Eq. (7), was solved by stepwise integration using trapezoidal discretization scheme [2].

Numerical simulation is performed for different cases listed in Table 1. These cases cover widespread ranges and can interpolate results in suitable correlations.

## RESULTS AND DISCUSION

Capture efficiency and deposition velocity are two important features in nanoparticle transport, which are sought in this study. In a microreactor, deposition can be a criterion for efficiency of a microreactive process.

Fig. 4 confirms the accuracy of LBM simulation as well as nanoparticle tracking by comparing the capture efficiency of nanoparticles in different diameters for case 1 in this study and Andarwa et al. [12]. The capture efficiency is defined as the ratio of the number of deposited nanoparticles to the total number entering the channel:

$$\text{Capture Efficiency (CE)} = \frac{\text{Number of deposited particles}}{\text{Number of injected particles}} \times 100 \quad (17)$$

As can be noticed, implementing the wall correction effect, hindered diffusion, reduces the capture efficiency.

Deposition location of nanoparticles in the presence of wall correction and without correction is shown for case 1 in Fig. 5. Channel length is divided into ten sections and the percent of deposited nanoparticles in each section to all deposited nanoparticles is obtained. As seen, the hindered diffusion reduces nanoparticle deposition along the channel. Due to domination of Brownian force, the smaller nanoparticles show more tendencies to deposit in the inlet of the channel, while in the larger ones, the drag force transfers the nanoparticles along the channel and deposition is uniform. Further, Fig. 5 indicates particle coating density differs at various dis-

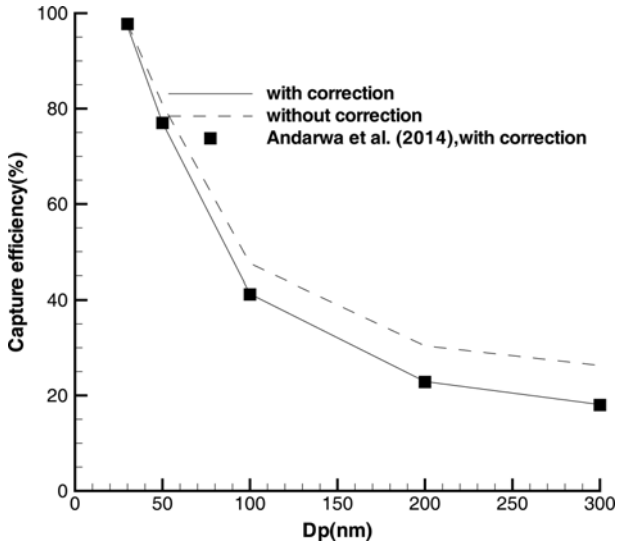


**Fig. 4. Variation in the capture efficiency with nanoparticle diameters for Case 1 and comparing the results with Andarwa et al. (2014).**

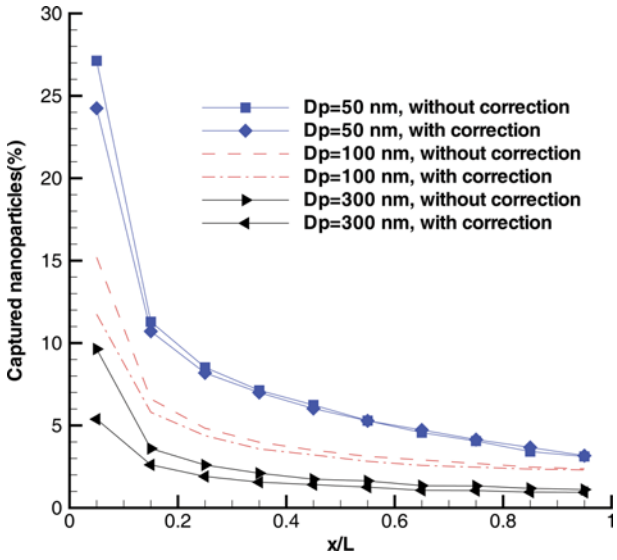


**Fig. 5. Deposition location along the channel for Case 1.**

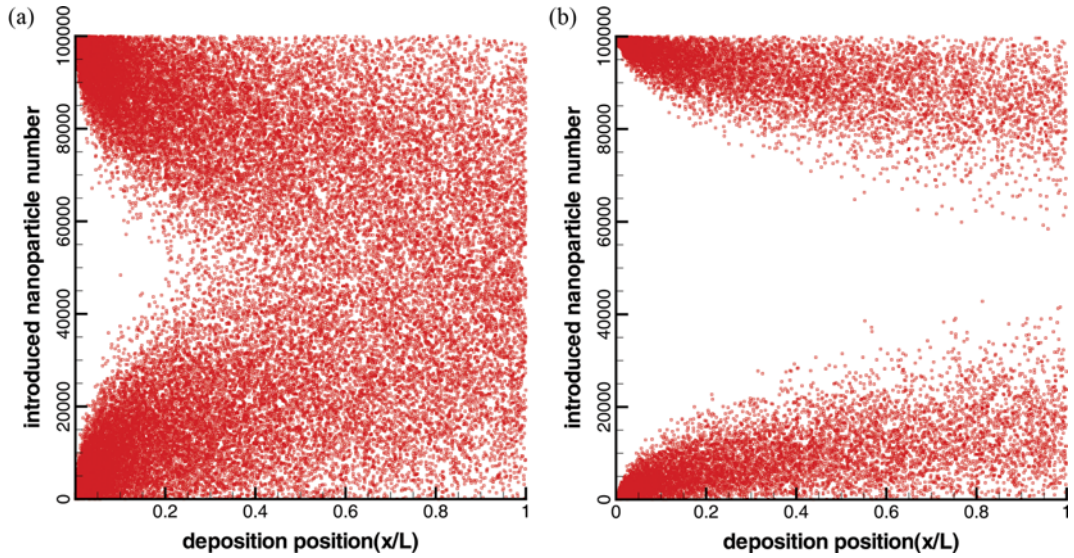


**Fig. 6. Deposition position of all introduced nanoparticles along the channel considering wall correction effect for Case 1, (a) for 100 nm and (b) for 300 nm nanoparticles.**

tances from the inlet section.

Fig. 6 depicts the deposition position of 100 (a) and 300 nm (b) nanoparticles in case 1 along the microchannel. Introduced nanoparticles are numbered from 1 to 100000 in near the bottom to near the upper wall. Comparison of Fig. 6(a) and (b) indicates that escape of the nanoparticle is more possible when the size is increased. In addition, in both figures the core nanoparticles have a much greater chance to escape from the channel due to increasing drag force in that region and farther away from the wall. Hence deposition is sensitive to the injection style especially for larger nanoparticles. As mentioned earlier, the presented results in this study are for uniform distribution injection.

Fig. 7 illustrates deposition velocity of different nanoparticles diameter, namely 30 and 100 nm in case 1. Deposition velocity is expressed as the particle flux to the walls divided by the particle number suspended in the duct in that time as [32]:

$$V_d(t)=\frac{N_{deposited@\Delta t}H}{N_{suspended@t}\Delta t} \tag{18}$$

In which $N_{deposited@\Delta t}$ is the number of particles that deposited during the time interval, $\Delta t$ and $N_{suspended@t}$ is the number of suspended particles at the beginning of each time interval.

Deposition rate is the multiplication of the deposition velocity and nanoparticle concentration. Deposition velocity is affected by the fluid flow and nanoparticle characteristics, as well as surface-nanoparticle interaction.

In Fig. 7, the deposition velocity for smaller nanoparticles is generally greater than larger ones, due to greater Brownian force, and consequently more tendency of smaller nanoparticles for deposition. At early stage, the deposition velocity is higher, which is in accordance with Fig. 5. Wall effect decreases the deposition velocity and this effect is more obvious in greater nanoparticles because

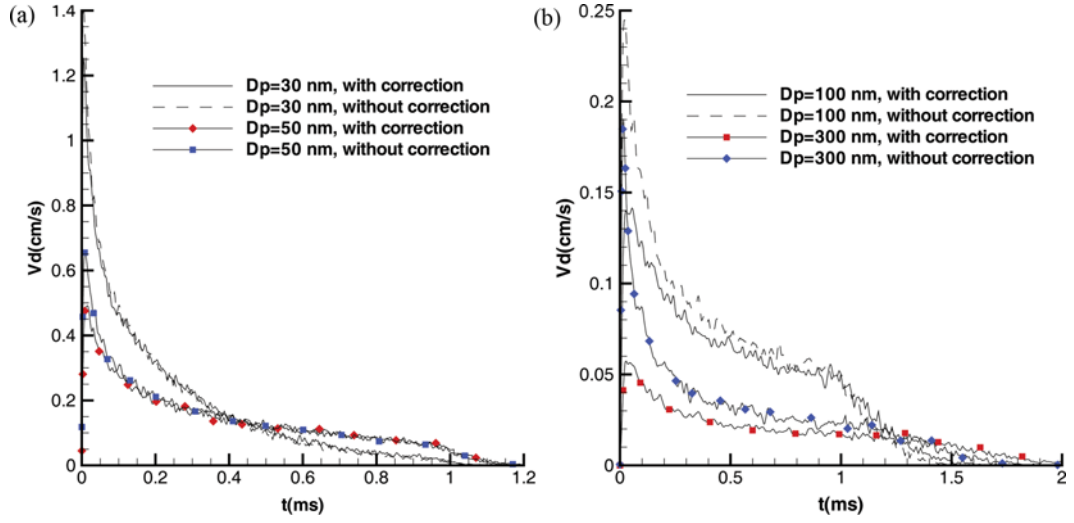


**Fig. 7. Variation in deposition velocity with time for Case 1(a): 30 and 50 nm (b): 100, 300 nm.**

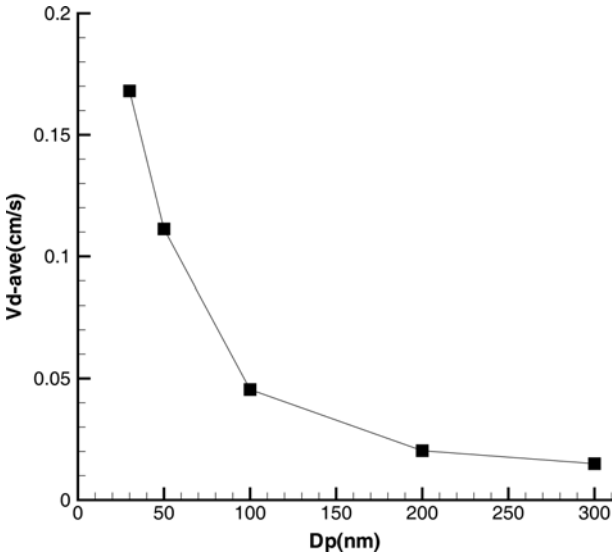


**Fig. 8. Time average deposition velocity considering wall correction effect for Case 1.**

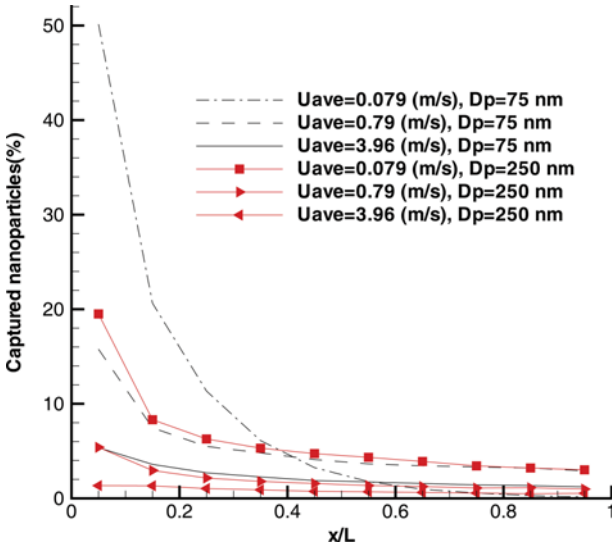


**Fig. 9. Deposition location considering wall correction effect for Cases 2, 3.**

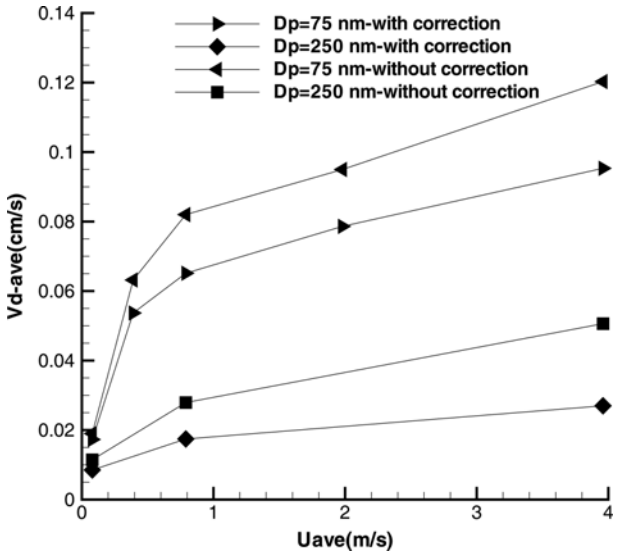


**Fig. 10. Time average deposition velocity for Case 2, 3.**

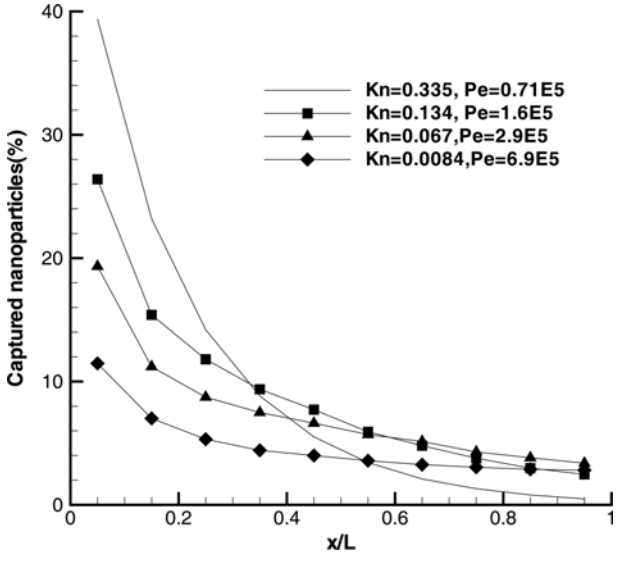


**Fig. 11. Deposition location for Case 4.**

of larger affected zone. Similarly, the time average deposition velocity ($V_{d-ave}$) is decreased with increasing nanoparticle diameter as seen in Fig. 8.

Deposition location of two different diameters, 75 and 250 nm nanoparticles in different fluid velocities, is shown in Fig. 9. Deposition mostly occurs in the leading edge of microchannel; it is sensitive to the nanoparticle diameter as well as fluid velocity. Increasing in the fluid velocity, the deposition follows a uniform pattern because of increasing drag force. This uniform pattern may be interesting for uniform coating.

The time average deposition velocity for cases 2, 3 is shown in Fig. 10. The time average deposition velocity for the smaller nanoparticles is greater than larger ones. In addition, increasing time average deposition velocity with increasing fluid velocity is because of decreasing time elapsed for traveling deposited nanoparticles. Moreover, the time average deposition velocity in the case of considering wall correction is significantly lower than without correction.

Up to now it was illustrated that considering the hindered diffusion, the wall effect, is important not only for capture efficiency but also in deposition location and deposition velocity. Therefore, the hindered diffusion should be considered as an effective factor in simulations.

To study the effect of the rarefaction on the nanoparticle transport, outlet pressure of fluid flow was changed and set to 0.2, 0.5, 1 and 8 atm in Case 4. Corresponding outlet Knudsen number and the Péclet number was obtained. The Péclet number is defined as the ratio of advection rate to diffusive rate of species:

$$Pe = U_{ave}L/D \;\&\; D = \frac{k_b T C_c(Kn_p)}{3\pi\mu d_p} \tag{19}$$

where D is the diffusion coefficient. Results of the deposition location are shown in Fig. 11. It is seen that deposition is increased with increasing the rarefaction.

Although, we might guess that the slip velocity of gaseous flow near boundaries is the cause of deviation in different rarefactions, the next discussion shows that this difference is mostly due to the change of the Brownian force a, favorable effect in deposition, to the drag force, unfavorable effect, ratio, as presented in Fig. 13.

Increasing the rarefaction leads to increasing the particle Knudsen number, $Kn_p$ so that the slip correction factor (Eq. (11)) is increased. Comparing Eqs. (10) and (12) results in:

$$F_B \propto \sqrt{\frac{1}{C_c(Kn_p)}},\ F_D \propto \frac{1}{C_c(Kn_p)} \tag{20}$$

Hence, increasing the rarefaction leads to more decreasing of the drag force in comparison with the Brownian force. Thus, the effect of Brownian diffusion is dominant on convective transfer. This can be expressed as decreasing Péclet number, and sorting of the results based on the Péclet number in Figs. 11 and 12 confirms this analysis. This finding indicates that rarefaction can be a serious problem in a colloguing microchannel. To prevent such effect, it may be preferred to classify nanoparticles and nanoparticles generated in higher operational pressure. Further, increasing the temperature shows the same effect and increases the deposition, as seen in Fig. 12. In addition, the Péclet number criterion again sorts the results successfully.

Fig. 13 compares the results of considering slip boundary condition (case 4, the precise flow field) for fluid flow with and without the wall correction effect as well as no slip effect. For the results of no slip, just no slip boundary condition is considered for the fluid velocity with the same fluid average velocity. As seen, up to Kn= 0.33 the results of slip and no slip are similar. Therefore, the main effect of Kn number is due to change of the forces acting on nanoparticles not the slip velocity of fluid flow near the wall. On the other hand, again the results of without the wall correction effect are overpredicted. However, with increasing Knudsen number, they converge.

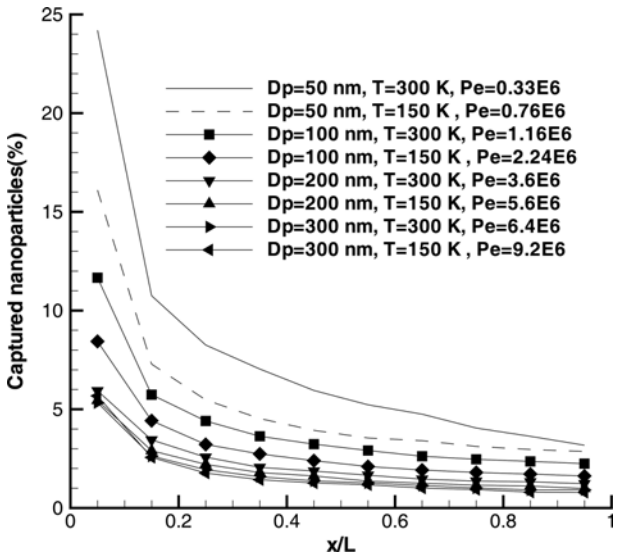


**Fig. 12. Deposition location in two temperatures (Case 5, Case 1).**

Correlation for the capture efficiency (CE) for all considered cases in Table 1 is sought. Fig. 14 shows the results can be correlated versus the deposition factor, which is:

$$\varphi = \frac{8}{3}\left(\frac{L}{2H}\right)^2 \frac{1}{Pe} \tag{21}$$

An acceptable correlation to fit all the results of cases 1-8 can be expressed with (see Fig. 14, Table 2):

$$CE = a\exp(b\,\varphi) + c\exp(d\,\varphi) \tag{22}$$

To seek a correlation for the time average deposition velocity, more details are needed to be considered. Using a non-dimensional average Sherwood number as,

$$Sh_{avg} = \frac{V_{d-ave} d_p}{D} \tag{23}$$

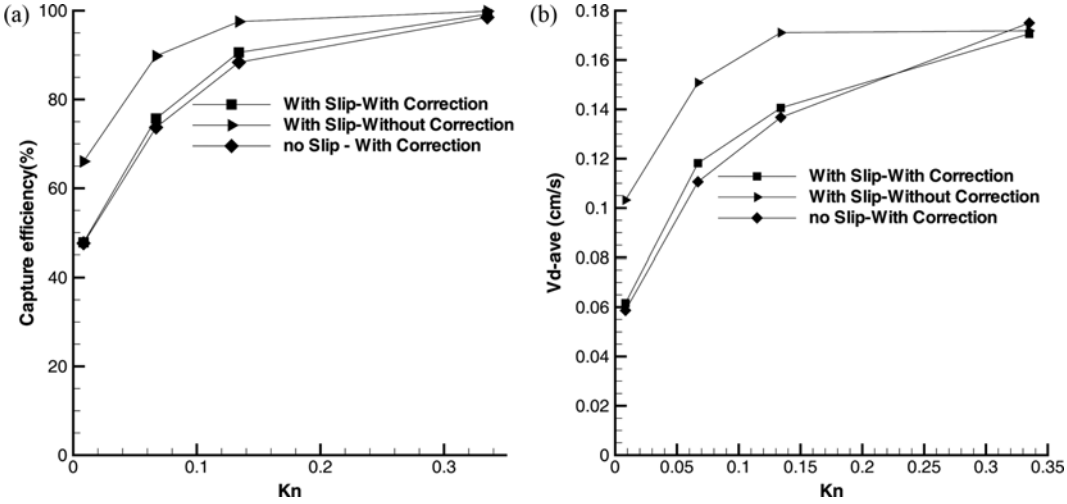


**Fig. 13. Capture efficiency (a) and time average deposition velocity (b) for Case 4 (with slip) with and without wall correction and corresponding no slip fluid velocity profile.**

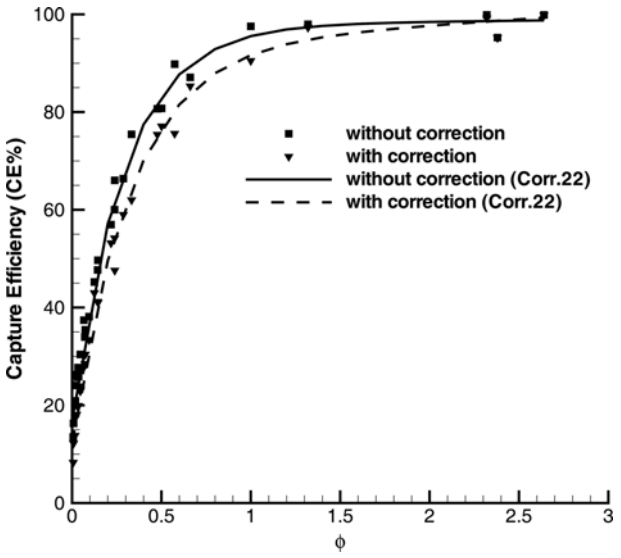


**Fig. 14. Capture efficiency for all cases (1-8) with and without correction effect and fitted curves.**

**Table 2. Constant for correlation 22**

| Constant | Without correction | With correction |
|---|---|---|
| a | 97.75 | 93.29 |
| b | 0.003928 | 0.02382 |
| c | −80.89 | −80.99 |
| d | −3.439 | −3.038 |

The results can be correlated versus the modified Péclet number as:

$$Pe_v = \frac{3U_{ave}d_p^3}{16H^2D} \tag{24}$$

An acceptable correlation to fit all the results of cases 1-8 can be expressed as (see Fig. 15, Table 3):

$$Sh_{avg} = aX_{Sh} + b \text{ where } X_{Sh} = \left(\frac{2HPe_v}{9L}\right)^{1/3} \tag{25}$$

Note that the wall correction effect is significant, especially for the average Sherwood number.

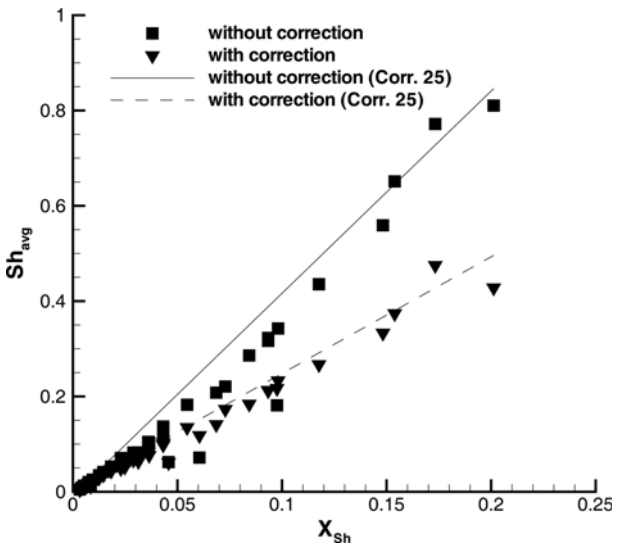


**Fig. 15. Average Sherwood number for all cases (1-8) with and without correction effect and fitted curves.**

**Table 3. Constant for correlation 25**

| Constant | Without correction | With correction |
|---|---|---|
| a | 4.243 | 2.449 |
| b | −0.007986 | 0.003456 |

## CONCLUSION

Applicability of LBM-LAG for simulation of nanoparticle transport in slip and early transient regime was discussed. The influence of the near-wall corrections on the nanoparticle transport as well as the rarefaction effects in microchannels was investigated. The wall correction effect on the capture efficiency, the deposition location, and the deposition velocity were shown to be significant. In fact, the hindered diffusion decreased the nanoparticle tendency to deposit and led to smaller capture efficiency and deposition velocity. Increasing the rarefaction increases tendency of nanoparticles deposition, which could be a serious problem in microchannel applications. Higher operating pressure led to decrease in deposition, which is noticeable for the nanoparticle handling in microchannel. For the smaller nanoparticles, deposition occurred in the leading edge of microchannel, while for the greater one became more uniformly along the channel. Time average deposition velocity increased for the smaller nanoparticles and higher fluid velocities. The proposed correlations of the capture efficiency and time average deposition velocity are capable of predicting parameters for the considered geometry. These findings could be important in the nanoparticle handling in the gaseous microchannel flow and filtration process.

## REFERENCES

1. O. M. Rahimi-Gorji, O. Pourmehran, M. Gorji-Bandpy and T. B. Gorji, *J. Mol. Liq.*, **209**, 121 (2015).
2. O. Pourmehran, M. Rahimi-Gorji, M. Gorji-Bandpy and T. B. Gorji, *J. Magn. Magn. Mater.*, **393**, 380 (2015).
3. O. Pourmehran, T. B. Gorji and M. Gorji-Bandpy, *Biomech. Model. Mechanobiol.*, **15**, 1355 (2016).
4. J. Tu, K., Inthavong and G. Ahmadi, *Computational fluid and particle dynamics in the human respiratory system*, 1st Ed., Springer Science & Business Media (2012).
5. L. H. Hung and A. P. Lee, *J. Med. Biol. Eng.*, **27**(1), 1 (2007).
6. N. Kockmann, S. Dreher, M. Engler and P. Woias, *Chem. Eng. J.*, **135**, S121 (2008).
7. J. S. Marshall, *J. Aerosol Sci.*, **38** (3), 333 (2007).
8. R. J. Yang, J. H. Hou, Y. N. Wang, C. H. Lin and L. M. Fu, *Biomicrofluidics*, **6**(3), 34110 (2012).
9. V. Ansari, A. S. Goharrizi, S. Jafari and B. Abolpour, *Comput. Fluids*, **108**, 170 (2015).

10. H. Basagaoglu, S. Allwein, S. Succi, H. Dixon, T. J. Carrola and S. Stothoff, *Microfluid. Nanofluid.*, **15**(6), 785 (2013).
11. H. Afshar, M. Shams, S. M. M. Nainian and G. Ahmadi, *Int. Commun. Heat Mass.*, **36**, 1060 (2009).
12. S. Andarwa, H. Basirat Tabrizi and G. Ahmadi, *Particuology*, **16**, 84 (2014).
13. A. Li and G. Ahmadi, *Aerosol Sci. Technol.*, **16**(4), 209 (1992).
14. E. E. Michaelides, *J. Fluids Eng.*, **138**(5), 51303 (2016).
15. E. Katelhon, S. V. Sokolov and R. G. Compton, *Sens. Actuat. B Chem.*, **234**, 420 (2016).
16. Z. Adamczyk and T. G. M. Van de Ven, *J. Colloid Interface Sci.*, **80**(2), 340 (1981).
17. M. Elimelech, J. Gregory and X. Jia, *Particle deposition and aggregation: measurement, modelling and simulation*, Butterworth-Heinemann (2013).
18. J. D. Park, J. S. Myung and K. H. Ahn, *Korean J. Chem. Eng.*, **33**(11), 3069 (2016).
19. S. Kandlikar, S. Garimella, D. Li, S. Colin and M. R. King, *Heat transfer and fluid flow in minichannels and microchannels*, Elsevier (2005).
20. X. J. Yue, Z. H. Wu, Y. S Ba, Y. J. Lu, Z. P. Zhu and C. D. Ba, *Int. J. Mod. Phys. C*, **26**(04), 1550037 (2015).
21. H. Wang, H. Zhao, Z. Guo, Y. He and C. Zheng, *J. Comp. Phys.*, **239**, 57 (2013).
22. Q. Zou and X. He, *Phys. Fluids*, **9**(6), 1591 (1997).
23. S. Succi, *Phys. Rev. Lett.*, **89**(6), 064502 (2002).
24. A. J. Goldman, R. G. Cox and H. Brenner, *Chem. Eng. Sci.*, **22**(4), 637 (1967).
25. A. J. Goldman, R. G. Cox and H. Brenner, *Chem. Eng. Sci.*, **22**(4), 653 (1967).
26. M. A. Bevan and C. D. Prieve, *J. Chem. Phys.*, **113**(3), 1228 (2000).
27. P. Huang, J. S. Guasto and K. S. Breuer, *J. Fluid Mech.*, **637**, 241 (2009).
28. B. Lin, J. Yu and S. A. Rice, *Phys. Rev. E*, **62**(3), 3909 (2000).
29. J. H. Kim, G. W. Mulholland, S. R. Kukuck and D. Y. Pui, *J. Res. Natl. Inst. Stan.*, **110**(1), 31 (2005).
30. P. G. T. Saffman, *J. Fluid Mech.*, **22**(2), 385 (1965).
31. M. Sommerfeld, *Int. J. Multiph. Flow*, **29**(4), 675 (2003).
32. S. Jung, D. J. Phares and A. R. Srinivasa, *Int. J. Multiph. Flow.*, **49**, 1 (2013).